



转动、堵塞效应和八极形变对U和Pu同位素对关联的影响

章骏 贺晓涛

Effects of Rotation, Blocking and Octupole Deformation on Pairing Correlations in the U and Pu Isotopes

ZHANG Jun, HE Xiaotao

在线阅读 View online: <https://doi.org/10.11804/NuclPhysRev.41.2023CNPC40>

引用格式:

章骏, 贺晓涛. 转动、堵塞效应和八极形变对U和Pu同位素对关联的影响[J]. 原子核物理评论, 2024, 41(1):178–183. doi: 10.11804/NuclPhysRev.41.2023CNPC40

ZHANG Jun, HE Xiaotao. Effects of Rotation, Blocking and Octupole Deformation on Pairing Correlations in the U and Pu Isotopes[J]. Nuclear Physics Review, 2024, 41(1):178–183. doi: 10.11804/NuclPhysRev.41.2023CNPC40

您可能感兴趣的其他文章

Articles you may be interested in

[\$^{235, 237}\text{Np}\$ 高自旋态的理论研究](#)

Theoretical Investigation of the High-spin States in $^{235, 237}\text{Np}$

原子核物理评论. 2022, 39(4): 413–420 <https://doi.org/10.11804/NuclPhysRev.39.2022047>

[能量密度泛函中不同对关联处理方式对原子核形变描述影响的探讨](#)

Effect of Different Pairing Correlations on the Description of Nuclear Deformations within Energy Density Functional Framework

原子核物理评论. 2020, 37(1): 26–33 <https://doi.org/10.11804/NuclPhysRev.37.2020006>

[超越平均场模型对Ba同位素链八极形状演化研究](#)

Beyond-mean-field Study of Octupole Shape Evolution in Neutron-deficient Ba Isotopes

原子核物理评论. 2019, 36(2): 144–150 <https://doi.org/10.11804/NuclPhysRev.36.02.144>

[精确可解对力模型下锕系元素同位素的裂变势垒](#)

Fission Barriers of Actinide Isotopes in the Exactly Solvable Pairing Model

原子核物理评论. 2023, 40(4): 502–510 <https://doi.org/10.11804/NuclPhysRev.40.2023013>

[A~80核区在束谱学研究进展](#)

Progress on the Spectroscopy in the A~80 Mass Region

原子核物理评论. 2020, 37(1): 11–17 <https://doi.org/10.11804/NuclPhysRev.37.2020001>

[基于壳模型对力加四极力研究sd和pf壳偶偶原子核](#)

Shell Model Study of Even-even sd and pf Shell Nuclei With the Pairing Plus Quadrupole-quadrupole Interaction

原子核物理评论. 2020, 37(3): 509–515 <https://doi.org/10.11804/NuclPhysRev.37.2019CNPC10>

Article ID: 1007-4627(2024)01-0178-06

Effects of Rotation, Blocking and Octupole Deformation on Pairing Correlations in the U and Pu Isotopes

ZHANG Jun¹, HE Xiaotao^{2,†}

(1. College of Physics, Nanjing University of Aeronautics and Astronautics, Nanjing 210016, China;

2. College of Materials Science and Technology, Nanjing University of Aeronautics and Astronautics, Nanjing 210016, China)

Abstract: By including octupole correlations in the Nilsson potential, the ground-state rotational bands in the reflection-asymmetric (RA) nuclei are investigated by using the cranked shell model (CSM) with the monopole and quadrupole pairing correlations treated by a particle-number-conserving (PNC) method. The experimental kinematic moments of inertia (MoIs) for alternating-parity bands in the even-even nuclei $^{236,238}\text{U}$ and $^{238,240}\text{Pu}$, as well as parity-doublet bands in the odd- A nuclei ^{237}U and ^{239}Pu are reproduced well by the PNC-CSM calculations. The higher $J^{(1)}$ for the intrinsic $s=-i$ bands in ^{237}U and ^{239}Pu , compared with the $s=+1$ bands in the neighboring even-even nuclei $^{236,238}\text{U}$ and $^{238,240}\text{Pu}$, can be attributed to the pairing gap reduction due to the Pauli blocking effect. The gradual increase of $J^{(1)}$ versus rotational frequency can be explained by the pairing gap reduction due to the rotation. The MoIs of reflection-asymmetric nuclei are higher than those of reflection-symmetric (RS) nuclei at low rotational frequency. Moreover, the inclusion of a larger octupole deformation ε_3 in the RA nuclei results in more significant pairing gap reduction compared with the RS nuclei.

Key words: octupole correlations; cranked shell model; particle-number-conserving method; alternating-parity bands; parity-doublet bands; pairing correlations

CLC number: O571.53 **Document code:** A **DOI:** 10.11804/NuclPhysRev.41.2023CNPC40

0 Introduction

The typical features for octupole correlations in the ground-state reflection-asymmetric (RA) nuclei are the occurrence of alternating-parity bands in the even-even nuclei and parity-doublet bands in the odd- A nuclei^[1]. These correlations in nuclei arise from the octupole-octupole interaction between single-particle states with differences in angular momentum $\Delta l = \Delta j = 3$. In the light actinide mass region, the proton Fermi surface lies between $f_{7/2}$ and $i_{13/2}$ orbitals, while the neutron Fermi surface lies between $g_{9/2}$ and $j_{15/2}$ orbitals in nuclei with proton number $Z \approx 88$ and neutron number $N \approx 134$. Since the proximity of these levels, strong octupole coupling lead to intrinsic reflection asymmetric shapes in the ground-state nuclei.

In the actinide mass region, most odd- A and even-even nuclei behave striking features of octupole correlations in the experiment^[2-6]. The rotational behaviors of the yrast and negative-parity bands in $^{236,237,238}\text{U}$ and those in $^{238,239,240}\text{Pu}$ exhibit significant differences, which is due to variations in octupole correlation strength^[7-11]. In terms of theoretical investigations, many approaches have been de-

veloped to describe the octupole correlations in the reflection-asymmetric nuclei. These include reflection-asymmetric mean-field approach^[12], cluster model^[13], vibrational approach^[14], reflection asymmetric shell model^[15], and cranked shell model^[16].

In the present work, the cranked shell model (CSM) with the pairing correlations treated by a particle-number-conserving (PNC) method is developed to investigate the alternating-parity bands in even-even nuclei $^{236,238}\text{U}$ and $^{238,240}\text{Pu}$, as well as the parity-doublet bands in odd- A nuclei ^{237}U and ^{239}Pu . In the PNC method, the CSM Hamiltonian is diagonalized directly in the truncated Fock space. Thus, the particle number is conserved exactly and the Pauli blocking effect is taken into account spontaneously. The effects of rotation, Pauli blocking, and octupole deformation on the pairing correlations in U and Pu isotopes have been investigated in detail by the PNC-CSM method.

1 Theoretical framework

In the framework of the cranked shell model, the Hamiltonian of an axially deformed nucleus is^[17-20]

Received date: 29 Jul. 2023; **Revised date:** 29 Feb. 2024

Foundation item: National Natural Science Foundation of China (U2032138, 11775112)

Biography: ZHANG Jun(1990-), Hefei, Anhui Province, Ph.D student, working on nuclear structure; E-mail: zhangjun3069@nuaa.edu.cn

† **Corresponding author:** HE Xiaotao, E-mail: hext@nuaa.edu.cn

$$H_{\text{CSM}} = H_{\text{Nil}} - \omega J_x + H_p(0) + H_p(2), \quad (1)$$

where $H_{\text{Nil}} = \sum h_{\text{Nil}}(\varepsilon_2, \varepsilon_3, \varepsilon_4)$ is the Nilsson Hamiltonian, in which the quadrupole (ε_2), octupole (ε_3) and hexadecapole (ε_4) deformation parameters are included^[16, 21]. $-\omega J_x$ is the Coriolis interaction with the rotational frequency ω about the x axis (perpendicular to the symmetry z axis here).

When $\omega = 0$, the single-particle Hamiltonian h_{Nil} has nonzero matrix elements of Y_{30} between different shell N . Since $p = (-1)^N$, the parity is no longer a good quantum number, but Ω (the single-particle angular momentum projection on the symmetry axis) is still a good quantum number. However, when $\omega \neq 0$, the symmetry with respect to the reflection through plane yoz , S_x operator, still holds. The single-particle orbitals can be labeled with the simplex quantum number s (the eigenvalues of S_x operator, $s = \pm i$).

The pairing includes the monopole and quadrupole pairing correlations,

$$H_p(0) = -G_0 \sum_{\xi\eta} a_{\xi}^{\dagger} a_{\xi}^{\dagger} a_{\eta} a_{\eta}, \quad (2)$$

$$H_p(2) = -G_2 \sum_{\xi\eta} q_2(\xi) q_2(\eta) a_{\xi}^{\dagger} a_{\xi}^{\dagger} a_{\eta} a_{\eta}, \quad (3)$$

where ξ is the eigenstates of the Nilsson Hamiltonian h_{Nil} , and $\bar{\xi}$ is the time-reversed states, $q_2(\xi) = \sqrt{16\pi/5} \langle \xi | r^2 Y_{20} | \xi \rangle$ is the diagonal element of the stretched quadrupole operator, and G_0 and G_2 are the effective strengths of monopole and quadrupole pairing interactions, respectively.

By diagonalizing the cranked shell model Hamiltonian in a sufficiently large cranked many-particle configuration (CMPC), a sufficiently accurate low-lying excited intrinsic wave function of the reflection-asymmetric nuclei are obtained as

$$|\psi\rangle = \sum_i C_i |i\rangle, \quad (4)$$

where $|i\rangle = |\mu_1 \mu_2 \cdots \mu_n\rangle$ is a CMPC for an n -particle system, and $\mu_1 \mu_2 \cdots \mu_n$ are the occupied cranked Nilsson orbitals. Each configuration $|i\rangle$ is characterized by the simplex s_i ,

$$s_i = s_{\mu_1} s_{\mu_2} \cdots s_{\mu_n}, \quad (5)$$

where s_{μ} is the simplex of the particle occupying in orbital μ . The kinematic moment of inertia (MoI) of eigenstate $|\psi\rangle$ can be written as

$$J^{(1)} = \frac{\langle \psi | J_x | \psi \rangle}{\omega}. \quad (6)$$

Experimentally, the rotational band with simplex quantum number s is characterized by spin states I of alternating parity^[22]

$$p = s e^{-i\pi I}. \quad (7)$$

Therefore for reflection-asymmetric systems with even number of nucleons we have

$$s = +1, \quad I^p = 0^+, 1^-, 2^+, 3^-, \cdots, \quad (8)$$

$$s = -1, \quad I^p = 0^-, 1^+, 2^-, 3^+, \cdots, \quad (9)$$

while for systems with odd number of nucleons we have

$$s = +i, \quad I^p = 1/2^+, 3/2^-, 5/2^+, 7/2^-, \cdots, \quad (10)$$

$$s = -i, \quad I^p = 1/2^-, 3/2^+, 5/2^-, 7/2^+, \cdots. \quad (11)$$

The moments of inertia for alternating parity bands can be expressed as

$$J_p^{(1)} = \frac{\langle \psi | J_x | \psi \rangle}{\omega} - \frac{1}{2} p \Delta J^{(1)}(\omega), \quad (12)$$

where $|\psi\rangle$ is the parity-independent wave function with the rotational frequency ω obtained by the PNC-CSM method. The $\Delta J^{(1)}(\omega)$ is the parity splitting of the moments of inertia in the experimental alternating-parity bands, which can be obtained by

$$\Delta J^{(1)}(\omega) = J_-^{(1)}(\omega) - J_+^{(1)}(\omega) \quad (13)$$

in which $J_-^{(1)}(\omega)$ and $J_+^{(1)}(\omega)$ are the experimental MoIs of the negative and positive parity rotational bands corresponding to the rotational frequency ω .

2 Results and Discussions

2.1 Parameters

In this work, the Nilsson parameters (κ, μ) are taken from Ref. [23]. The deformations ε_2 , ε_3 , and ε_4 are input parameters in the PNC-CSM method. The values of ε_2 and ε_4 are chosen close to the calculated deformations of the ground states in the actinide region^[24]. The ε_3 values used in this work are chosen by fitting the experimental MoIs and alignments of the ground-state bands in the U and Pu isotopes. The deformation parameters ($\varepsilon_2, \varepsilon_3, \varepsilon_4$) used in our PNC-CSM calculations are (0.200, 0.110, -0.055), (0.220, 0.130, -0.040), (0.228, 0.025, -0.065), and (0.230, 0.010, -0.045) for even-even nuclei ^{236}U , ^{238}U , ^{238}Pu , and ^{240}Pu , respectively. The deformation parameters of odd- A nuclei ^{237}U and ^{239}Pu are taken as the average of the neighboring even-even nuclei.

The effective pairing strengths G_0 and G_2 , in principle, can be determined by the odd-even differences in nuclear binding energies. The values are connected with the dimensions of the truncated cranked many-particle configuration space. For even-even nuclei $^{236, 238}\text{U}$ and $^{238, 240}\text{Pu}$, the effective monopole and quadrupole pairing strengths are $G_{0p} = 0.25$ MeV, $G_{2p} = 0.03$ MeV and $G_{0n} = 0.25$ MeV, $G_{2n} = 0.015$ MeV for protons and neutrons, respectively. For odd- A nuclei ^{237}U and ^{239}Pu , the neutron pairing

strengths are little smaller than those in even-even nuclei. For all nuclei studied in this work, the CMPC space is constructed in the proton $N = 5, 6$ and neutron $N = 6, 7$ shells. The dimensions of the CMPC space are about 1 000 for both protons and neutrons.

2.2 Moments of inertia

Figure 1 shows the experimental and calculated kinematic moments of inertia $J^{(1)}$ for the alternating-parity bands ($s = +1$) in even-even nuclei $^{236, 238}\text{U}$ and $^{238, 240}\text{Pu}$, and parity-doublet bands ($s = \pm i$) in odd- A nuclei ^{237}U and ^{239}Pu . The experimental data for the negative (positive) parity bands are denoted by green solid (open) circles. The PNC-CSM calculations in the reflection-asymmetric nuclei are denoted by black solid lines. After considering the parity spitting of Eqs. (12) and (13), the $J^{(1)}$ of negative and positive parity bands are denoted by dash-dotted and dotted lines, respectively. The PNC-CSM calculations in the reflection-symmetric (RS) nuclei (without ε_3 deformation) are shown by red dashed lines. It can be seen that the experimental moments of inertia versus the rotational frequency $\hbar\omega$ are reproduced very well by the PNC-CSM calculations. As shown in Figs. 1(b), 1(c), 1(f), and 1(g), there are simplex splittings between $s = +i$ and $s = -i$ partner bands (solid black lines) at $\hbar\omega < 0.10$ MeV in both odd- A nuclei ^{237}U and ^{239}Pu .

From Fig. 1, we can see that the moments of inertia $J^{(1)}$ gradually increase with rotational frequency in all nuclei. For intrinsic rotational band in ^{236}U , the calculated difference in MoIs $\delta J/J$ with increasing ω is

$$\frac{\delta J}{J} = \frac{J(^{236}\text{U}, \hbar\omega = 0.30 \text{ MeV}) - J(^{236}\text{U}, \hbar\omega = 0)}{J(^{236}\text{U}, \hbar\omega = 0)} \approx 87.3\%. \quad (14)$$

It can be seen that the $J^{(1)}$ of intrinsic rotational band in ^{236}U increase about 87% at the frequency $\hbar\omega = 0.30$ MeV compared with that at the bandhead. For other nuclei, the results are very similar, and will not be shown here.

At the bandhead, the calculated odd-even differences in MoIs $\delta J/J$ between the intrinsic $s = -i$ rotational bands in odd- A nuclei ^{237}U and ^{239}Pu and those in the neighboring even-even nuclei ^{236}U and ^{238}Pu are:

$$\frac{\delta J}{J} = \frac{J(^{237}\text{U}, \text{RA}) - J(^{236}\text{U}, \text{RA})}{J(^{236}\text{U}, \text{RA})} \approx 61.0\%,$$

$$\frac{\delta J}{J} = \frac{J(^{239}\text{Pu}, \text{RA}) - J(^{238}\text{Pu}, \text{RA})}{J(^{238}\text{Pu}, \text{RA})} \approx 49.6\%. \quad (15)$$

Therefore, the higher $J^{(1)}$ in the odd- A nuclei compared with those in the neighboring even-even nuclei mainly attribute to the blocking of unpaired neutron.

Furthermore, as shown in Fig. 1, the calculated MoIs of the intrinsic rotational bands in the reflection-asymmetric nuclei are obviously higher than those in reflection-symmetric nuclei. At the bandhead, the calculated differences in MoIs $\delta J/J$ between the RA and RS rotational bands for the U isotopes are:

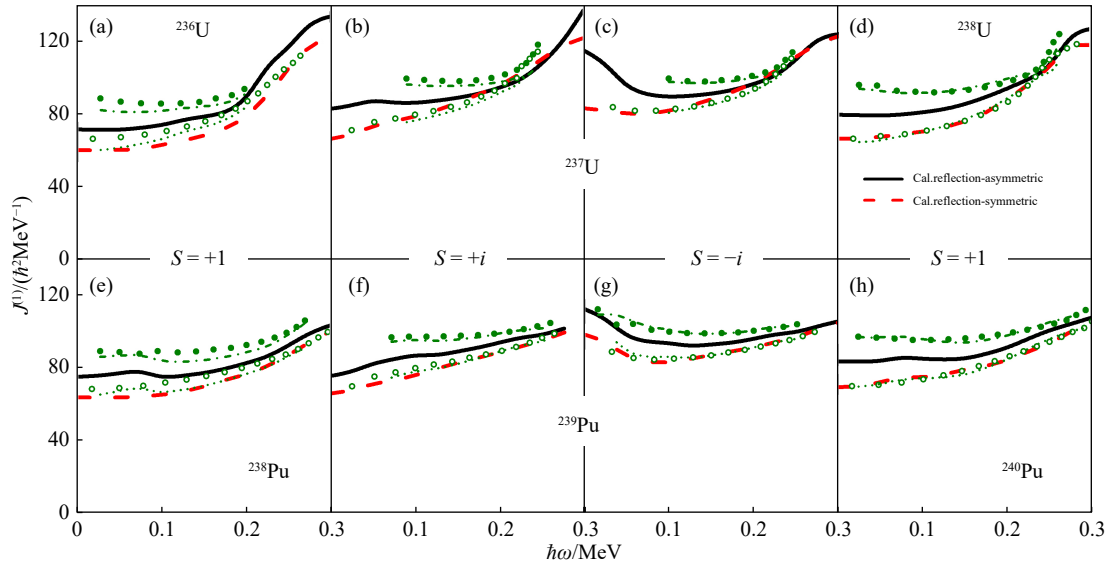


Fig. 1 The experimental and calculated kinematic moments of inertia $J^{(1)}$ for the alternating-parity bands in even-even nuclei $^{236, 238}\text{U}$ and $^{238, 240}\text{Pu}$, and parity-doublet bands in odd- A nuclei ^{237}U and ^{239}Pu . The experimental data for the negative (positive) parity bands are denoted by solid (open) circles. The PNC-CSM calculations in the reflection-asymmetric nuclei are denoted by black solid lines. After considering the parity spitting of Eqs. (12) and (13), the negative and positive parity bands are denoted by dash-dotted and dotted lines, respectively. The PNC-CSM calculations in the reflection-symmetric nuclei (without ε_3 deformation) are shown by red dashed lines. The ε_3 deformation parameters for ^{236}U , ^{237}U , and ^{238}U are 0.110, 0.071, and 0.130, and those for ^{238}Pu , ^{239}Pu , and ^{240}Pu are 0.025, 0.010, and 0.010. (color online)

$$\begin{aligned}\frac{\delta J}{J} &= \frac{J(^{236}\text{U, RA}) - J(^{236}\text{U, RS})}{J(^{236}\text{U, RS})} \approx 18.7\%, s = +1, \\ \frac{\delta J}{J} &= \frac{J(^{237}\text{U, RA}) - J(^{237}\text{U, RS})}{J(^{237}\text{U, RS})} \approx 24.7\%, s = +i, \\ \frac{\delta J}{J} &= \frac{J(^{237}\text{U, RA}) - J(^{237}\text{U, RS})}{J(^{237}\text{U, RS})} \approx 37.8\%, s = -i, \\ \frac{\delta J}{J} &= \frac{J(^{238}\text{U, RA}) - J(^{238}\text{U, RS})}{J(^{238}\text{U, RS})} \approx 19.7\%, s = +1, \quad (16)\end{aligned}$$

and the calculated results for the Pu isotopes are:

$$\begin{aligned}\frac{\delta J}{J} &= \frac{J(^{238}\text{Pu, RA}) - J(^{238}\text{Pu, RS})}{J(^{238}\text{Pu, RS})} \approx 17.7\%, s = +1, \\ \frac{\delta J}{J} &= \frac{J(^{239}\text{Pu, RA}) - J(^{239}\text{Pu, RS})}{J(^{239}\text{Pu, RS})} \approx 14.3\%, s = +i, \\ \frac{\delta J}{J} &= \frac{J(^{239}\text{Pu, RA}) - J(^{239}\text{Pu, RS})}{J(^{239}\text{Pu, RS})} \approx 14.1\%, s = -i, \\ \frac{\delta J}{J} &= \frac{J(^{240}\text{Pu, RA}) - J(^{240}\text{Pu, RS})}{J(^{240}\text{Pu, RS})} \approx 20.0\%, s = +1. \quad (17)\end{aligned}$$

We can see that the differences in MoIs $\delta J/J$ in the U isotopes are almost larger than those in the Pu isotopes. In this work, the ε_3 deformation parameters for ^{236}U , ^{237}U , and ^{238}U are 0.110, 0.071, and 0.130, while those for ^{238}Pu , ^{239}Pu , and ^{240}Pu are 0.025, 0.010, and 0.010. Thus, it can

be seen clearly that ε_3 deformation gives a very significant contribution to the variation of $J^{(1)}$.

In order to have a more clear understanding of the variation of $J^{(1)}$, we study the effects of rotation, blocking and octupole deformation on the pairing correlations in the U and Pu isotopes in detail.

2.3 Pairing correlations

The nuclear pairing gap is defined as^[25]

$$\tilde{\Delta} = G_0 \left[-\frac{1}{G_0} \langle \psi | H_p | \psi \rangle \right]^{1/2}. \quad (18)$$

Figure 2 shows the calculated proton and neutron pairing gaps $\tilde{\Delta}$ versus the rotational frequency $\hbar\omega$ for the alternating-parity bands in even-even nuclei $^{236,238}\text{U}$ and $^{238,240}\text{Pu}$, and the parity-doublet bands in odd- A nuclei ^{237}U and ^{239}Pu . The effective pairing strengths are the same for the reflection-asymmetric and reflection-symmetric nuclei in the PNC-CSM calculations. As shown in Fig. 2, the pairing gaps $\tilde{\Delta}$ in the reflection-asymmetric nuclei are almost smaller than those in the reflection-symmetric nuclei for both protons and neutrons. The pairing gaps decrease with increasing rotation frequency $\hbar\omega$, and significantly decrease for the neutrons in the odd- A nuclei ^{237}U and ^{239}Pu .

The calculated pairing gap reductions with increasing rotational frequency in the reflection-asymmetric nuclei ^{236}U are:

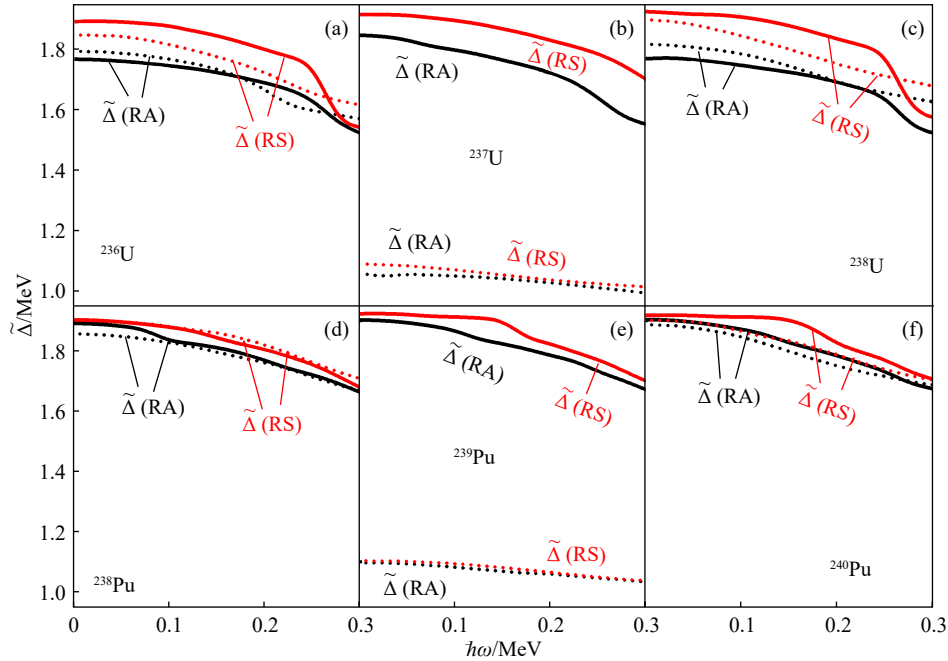


Fig. 2 The calculated proton and neutron pairing gaps $\tilde{\Delta}$ versus the rotational frequency $\hbar\omega$ for the alternating-parity bands in even-even nuclei $^{236,238}\text{U}$ and $^{238,240}\text{Pu}$, and parity-doublet bands in odd- A nuclei ^{237}U and ^{239}Pu . The PNC-CSM calculations in the reflection-asymmetric nuclei are denoted by black lines, and those in the reflection-symmetric nuclei (without ε_3 deformation) are denoted by red lines. The solid and dotted lines are for protons and neutrons, respectively. The ε_3 deformation parameters for ^{236}U , ^{237}U , and ^{238}U are 0.110, 0.071, and 0.130, and those for ^{238}Pu , ^{239}Pu , and ^{240}Pu are 0.025, 0.010, and 0.010. (color online)

$$\frac{\delta\tilde{\Delta}_p}{\tilde{\Delta}_p} = \frac{\tilde{\Delta}_p(^{236}\text{U}, \hbar\omega = 0.30\text{ MeV}) - \tilde{\Delta}_p(^{236}\text{U}, \omega = 0)}{\tilde{\Delta}_p(^{236}\text{U}, \omega = 0)} = 13.8\%,$$

$$\frac{\delta\tilde{\Delta}_n}{\tilde{\Delta}_n} = \frac{\tilde{\Delta}_n(^{236}\text{U}, \hbar\omega = 0.30\text{ MeV}) - \tilde{\Delta}_n(^{236}\text{U}, \omega = 0)}{\tilde{\Delta}_n(^{236}\text{U}, \omega = 0)} = 12.5\%. \quad (19)$$

The results are very similar for other nuclei, which are not shown here. For both protons and neutrons, it can be seen that the pairing gaps decrease by about 10% at the frequency $\hbar\omega = 0.30\text{ MeV}$ compared with those at the bandhead. These result in the gradual increase of $J^{(1)}$ versus rotational frequency in all nuclei.

Comparing Figs. 2(a), 2(d) and Figs. 2(b), 2(e), it is seen that the pairing gaps of neutrons decrease in the odd- A nuclei ^{237}U and ^{239}Pu . At the bandhead, the calculated neutron pairing gap reductions for these nuclei are:

$$\frac{\delta\tilde{\Delta}_n}{\tilde{\Delta}_n} = \frac{\tilde{\Delta}_n(^{237}\text{U}, \text{RA}) - \tilde{\Delta}_n(^{236}\text{U}, \text{RA})}{\tilde{\Delta}_n(^{236}\text{U}, \text{RA})} = 41.0\%,$$

$$\frac{\delta\tilde{\Delta}_n}{\tilde{\Delta}_n} = \frac{\tilde{\Delta}_n(^{239}\text{Pu}, \text{RA}) - \tilde{\Delta}_n(^{238}\text{Pu}, \text{RA})}{\tilde{\Delta}_n(^{238}\text{Pu}, \text{RA})} = 40.9\%. \quad (20)$$

We can see that the pairing gaps decrease about 40% in the odd- A nuclei compared with the neighboring even-even nuclei, which lead to higher $J^{(1)}$ for the $s = -i$ bands in these odd- A nuclei [see Figs. 1(a), 1(c), 1(e) and 1(g)].

At the bandhead, the calculated pairing gap reductions for ^{236}U with reflection-asymmetric deformation and reflection-symmetric deformation are:

$$\frac{\delta\tilde{\Delta}_p}{\tilde{\Delta}_p} = \frac{\tilde{\Delta}_p(^{236}\text{U}, \text{RA}) - \tilde{\Delta}_p(^{236}\text{U}, \text{RS})}{\tilde{\Delta}_p(^{236}\text{U}, \text{RS})} = 6.6\%,$$

$$\frac{\delta\tilde{\Delta}_n}{\tilde{\Delta}_n} = \frac{\tilde{\Delta}_n(^{236}\text{U}, \text{RA}) - \tilde{\Delta}_n(^{236}\text{U}, \text{RS})}{\tilde{\Delta}_n(^{236}\text{U}, \text{RS})} = 2.9\%, \quad (21)$$

and the calculated results for ^{238}Pu are:

$$\frac{\delta\tilde{\Delta}_p}{\tilde{\Delta}_p} = \frac{\tilde{\Delta}_p(^{238}\text{Pu}, \text{RA}) - \tilde{\Delta}_p(^{238}\text{Pu}, \text{RS})}{\tilde{\Delta}_p(^{238}\text{Pu}, \text{RS})} = 0.6\%,$$

$$\frac{\delta\tilde{\Delta}_n}{\tilde{\Delta}_n} = \frac{\tilde{\Delta}_n(^{238}\text{Pu}, \text{RA}) - \tilde{\Delta}_n(^{238}\text{Pu}, \text{RS})}{\tilde{\Delta}_n(^{238}\text{Pu}, \text{RS})} = 2.4\%. \quad (22)$$

We can see that the pairing gaps decrease in the reflection-asymmetric nuclei compared with the reflection-symmetric nuclei. Furthermore, the pairing gap reduction becomes even more significant with increasing the octupole deformation [see Figs. 2(a) and 2(c)]. Therefore, the octupole correlations give a certain effect on the increase of $J^{(1)}$ in the reflection-asymmetric nuclei. The results are very similar for other nuclei, which are not shown here.

3 Summary

The reflection-asymmetric nuclei $^{236,237,238}\text{U}$ and $^{238,239,240}\text{Pu}$ are investigated by the cranked shell model with pairing correlations treated by the particle-number-conserving method. The experimental moments of inertia of the alternating-parity bands in the even-even nuclei $^{236,238}\text{U}$ and $^{238,240}\text{Pu}$ and the parity-doublet bands in the odd- A nuclei ^{237}U and ^{239}Pu are reproduced well by the PNC-CSM calculations. The pairing gaps in these nuclei are significantly influenced by rotation, Pauli blocking, and octupole deformation. The gradual increases of $J^{(1)}$ versus rotational frequency in these nuclei are mainly due to the pairing gap reductions with increasing ω . The higher $J^{(1)}$ for the intrinsic $s = -i$ bands in the odd- A nuclei compared with the neighboring even-even nuclei can be attributed to the pairing gap reductions due to Pauli blocking effects. The $J^{(1)}$ of the intrinsic rotational bands in the RA nuclei are higher than those in the RS nuclei. Furthermore, a larger octupole deformation ε_3 in the RA nuclei results in more significant pairing gap reduction compared with the RS nuclei.

References:

- [1] AHMAD I, BUTLER P A. *Annu Rev Nucl Part Sci*, 1993, 43(1): 71.
- [2] LEVON A I, DE BOER J, LOEWE M, et al. *Eur Phys J A*, 1998, 2(1): 9.
- [3] LIANG C F, PARIS P, SHELIN R K, et al. *Phys Rev C*, 1998, 57: 1145.
- [4] ZAMFIR N V, KUSNEZOV D. *Phys Rev C*, 2003, 67: 014305.
- [5] BUCK B, MERCHANT A C, PEREZ S M. *J Phys G: Nucl Part Phys*, 2008, 35(8): 085101.
- [6] PARR E, SMITH J F, GREENLEES P T, et al. *Phys Rev C*, 2022, 105: 034303.
- [7] WARD D, ANDREWS H, BALL G, et al. *Nucl Phys A*, 1996, 600(1): 88.
- [8] WIEDENHÖVER I, JANSSENS R V F, HACKMAN G, et al. *Phys Rev Lett*, 1999, 83: 2143.
- [9] WANG X, JANSSENS R V F, CARPENTER M P, et al. *Phys Rev Lett*, 2009, 102: 122501.
- [10] ZHU S, CARPENTER M P, JANSSENS R V F, et al. *Phys Rev C*, 2010, 81: 041306.
- [11] SPIEKER M, BUCURESCU D, ENDRES J, et al. *Phys Rev C*, 2013, 88: 041303.
- [12] ROBLEDO L M, BERTSCH G F. *Phys Rev C*, 2011, 84: 054302.
- [13] CHEN X C, ZHAO J, XU C, et al. *Phys Rev C*, 2016, 94: 021301.
- [14] DOBROWOLSKI A, MAZUREK K, GÓŹDŹ A. *Phys Rev C*, 2018, 97: 024321.
- [15] CHEN Y S, GAO Z C. *Phys Rev C*, 2000, 63: 014314.
- [16] HE X T, LI Y C. *Phys Rev C*, 2020, 102: 064328.
- [17] ZENG J Y, CHENG T S. *Nucl Phys A*, 1983, 405(1): 1.
- [18] LIU S X, ZENG J Y, ZHAO E G. *Phys Rev C*, 2002, 66: 024320.
- [19] ZHANG Z H. *Nucl Phys A*, 2016, 949: 22.

- [20] HE X T, LI Y C. *Phys Rev C*, 2018, 98(6): 064314. 014324.
[21] ZHANG J, HE X T, LI Y C, et al. *Phys Rev C*, 2023, 107: 024305. [24] NILSSON S G, TSANG C F, SOBICZEWSKI A, et al. *Nucl Phys A*, 1969, 131(1): 1.
[22] NAZAREWICZ W, OLANDERS P. *Nucl Phys A*, 1985, 441(3): 420. [25] WU X, ZHANG Z H, ZENG J Y, et al. *Phys Rev C*, 2011, 83: 034323.
[23] ZHANG Z H, HE X T, ZENG J Y, et al. *Phys Rev C*, 2012, 85:

转动、堵塞效应和八极形变对 U 和 Pu 同位素对关联的影响

章骏¹, 贺晓涛^{2,†}

(1. 南京航空航天大学物理学院, 南京 210016;
2. 南京航空航天大学材料科学与技术学院, 南京 210016)

摘要: 通过在 Nilsson 势中引入八极关联, 基于推转壳模型 (CSM) 下处理对相互作用的粒子数守恒方法 (PNC), 研究了反射不对称原子核的基态转动带。PNC-CSM 的计算结果重现了轻锕系区偶偶核 $^{236,238}\text{U}$ 和 $^{238,240}\text{Pu}$ 的交替宇称带, 以及奇- A 核 ^{237}U 和 ^{239}Pu 的宇称双重带的转动惯量实验值。奇- A 核 ^{237}U 和 ^{239}Pu 的 $s=-i$ 内禀转动带的转动惯量较相邻偶偶核 $^{236,238}\text{U}$ 和 $^{238,240}\text{Pu}$ 的 $s=+1$ 转动带显著增加, 这主要归因于泡利堵塞效应导致中子体系的对关联衰减。U 和 Pu 同位素中, 转动惯量随着转动频率缓慢增加则是由于对关联随着角频率的增加而衰减所造成的。在低频率区, 反射不对称原子核的转动惯量明显高于相对应的反射对称原子核的转动惯量。并且与反射对称原子核相比, 较大的八极形变将导致反射不对称原子核体系的对关联衰减更加明显。

关键词: 八极关联; 推转壳模型; 粒子数守恒方法; 交替宇称带; 宇称双重带; 对关联

收稿日期: 2023-07-29; 修改日期: 2024-02-29

基金项目: 国家自然科学基金资助项目 (U2032138, 11775112)

† 通信作者: 贺晓涛, E-mail: hext@nuaa.edu.cn